

Verifying Operational Forecasts of Land-Sea Breeze and Boundary Layer

Mixing Processes

Ewan Short*

*School of Earth Sciences, and ARC Centre of Excellence for Climate Extremes, The University of
Melbourne, Melbourne, Victoria, Australia.*

Ben ?. Price

Bureau of Meteorology, Casuarina, Northern Territory, Australia

Derryn ?. Griffiths and Alexei ?. Hider

Bureau of Meteorology, Melbourne, Victoria, Australia

*Corresponding author address: School of Earth Sciences, The University of Melbourne, Melbourne, Victoria, Australia.

E-mail: shorte1@student.unimelb.edu.au

ABSTRACT

13 This paper presents a method for verifying the diurnally varying compo-
14 nent of the wind forecasts issued by the Australian Bureau of Meteorology.
15 These wind forecasts are based on model data that is then edited by human
16 forecasters. The model datasets most commonly used by Australian forecast-
17 ers for winds are those of the European Center for Medium-Range Weather
18 Forecasting (ECMWF) and the Australian Community Climate and Earth Sys-
19 tem Simulator (ACCESS). The methodology is applied to the coastal weather
20 stations across Australia over June, July and August 2018, at three different
21 spatial scales, on both a daily and seasonal basis. The results indicate that
22 while the Official forecast outperforms unedited ACCESS and ECMWF at
23 certain locations and times of day, it rarely outperforms both at once. The
24 causes of the differences in the performance of each dataset vary by location,
25 but can include biases in the direction at which the sea-breeze approaches the
26 coast, amplitude biases in the diurnal cycle, and disagreement as to whether
27 sea-breeze or boundary layer mixing processes contribute most to the diurnal
28 cycle. Furthermore, when winds are compared at small spatial scales on a
29 daily basis, ECMWF outperforms Official and ACCESS simply because its
30 coarser resolution creates less internal variability than Official or ACCESS.
31 These results have implications for both forecasting practice and verification
32 methodology.

33 1. Introduction

34 Modern weather forecasts are typically produced by models in conjunction with human fore-
35 casters. Forecasters working for the Australian Bureau of Meteorology (BoM) construct a seven
36 day forecast by loading model data into a software package called the Graphical Forecast Editor
37 (GFE), then editing this model data using tools within GFE. Is this also how things work at the
38 U.S National Weather Service and U.K. Met Office? Forecasters can choose which model to base
39 their forecast on, and refer to this as a choice of *model guidance*. Edits are typically made to
40 account for processes that are under-resolved at synoptic scale model resolutions, or to correct
41 known biases of the models being used. The resulting gridded forecast datasets are then provided
42 to the public through the BoM’s online MetEye data browser (Bureau of Meteorology 2019); the
43 gridded forecast datasets are also translated into text and icon forecasts algorithmically.

44 Australian forecasters generally make two types of edits to the surface wind fields on a routine
45 daily basis. The first is to edit the surface winds after sunrise at locations where the forecaster be-
46 lieves the model guidance is providing a poor representation of boundary layer mixing processes.
47 Boundary layer mixing occurs as the land surface heats up, producing an unstable boundary layer
48 which transports momentum downward to the “surface layer”, where winds are both weaker and
49 ageostrophically oriented due to surface friction (Lee 2018). The forecaster may edit both speed
50 and direction on the basis of climatological knowledge, theory or recent upper level wind sound-
51 ings from nearby stations. How do the boundary layer mixing tools in GFE currently work? While
52 I was in Darwin you essentially picked a height z and a percentage p , and the tool essentially
53 formed an average of the surface winds and winds at x weighted by p .

54 The second type of edit involves changing the afternoon and evening surface winds around those
55 coastlines where the forecaster believes the model guidance is resolving the sea-breeze poorly.

56 How do the sea-breeze tools in GFE currently work? While I was in Darwin you traced out the
57 relevant coastline graphically, chose a wind speed and a time, and GFE would add in winds perpen-
58 dicular to the traced coastline at this speed, and smoothly blend them in spatially and temporally.

59 The motivation for performing these edits

60 Two edits are commonly involves changing the surface wind fields near coastlines to try to rep-
61 resent sea-breezes more realistically. Forecasters invest time in making sea-breeze edits because
62 accurate predictions of near-surface winds are highly valued by a number of users, such as the
63 aviation and energy (Smith et al. 2009) industries. Accurate sea-breeze forecasts are also valuable
64 to environmental monitoring authorities, as these winds provide ventilation to coastal urban areas.

65 Assessing the accuracy of a weather forecast is a task far more nuanced than it might first appear.
66 For instance, attempting to assess the accuracy of a precipitation forecast by comparing the rainfall
67 amounts measured at an individual weather station to the closest grid point of a model prediction
68 will often give poor results. Although the synoptic drivers of convection are usually well predicted,
69 exactly where convective cells form, and where the most rain falls, is highly unpredictable. As
70 such, it is often appropriate to use “fuzzy” verification metrics which measure the agreement
71 between prediction and observation in a more indirect way. For instance, one approach known as
72 “upscaling” is to first average forecast and observational data over a given spatial domain before
73 calculating verification scores. Ebert (2008) provided a review of current “fuzzy verification”
74 methodologies, and a framework for how they can be used to determine the spatial scales at which
75 a given forecast has predictive skill.

76 Relatively few forecast verification studies have focused on near-surface winds, and the ones
77 that have generally only considered wind speeds. Pinson and Hagedorn (2012) performed a veri-
78 fication study of the ECMWF 10 m wind speeds across western Europe over December, January,
79 February 2008/09. First, they interpolated ECMWF model data onto the locations of weather

80 stations across Europe, then they compared the interpolated model data at these stations with the
81 station observations themselves. They found that the worst performing regions were coastal and
82 mountainous areas, and attributed this poor performance to the small scale processes, e.g. sea
83 and mountain breezes, that are underresolved at ECMWF's coarse 50km spatial resolution. They
84 noted that future work could better identify the effect of diurnal cycles on verification statistics by
85 considering forecasts at different times of day.

86 Lynch et al. (2014) also performed a verification study of ECMWF 10 m wind speed data, with
87 the goal of assessing skill at lead times of between 14 to 20 days. They compared ECMWF 32-
88 day forecast model wind speeds with gridded ERA-Interim wind speeds between 2008-12, with
89 both datasets analysed at a six hour temporal resolution. Before conducting the comparison, the
90 wind speed data were transformed into wind-speed "anomaly" data by first calculating the mean
91 wind speed at 0000, 0600, 1200 and 1800 UTC for each calendar day from the entire ERA-Interim
92 record, and from a 20 year ECMWF 32-day model hindcast, then subtracting these means from the
93 ERA-Interim and ECMWF 32-day model data respectively. Wind speed anomaly data was used
94 so that stable seasonal and diurnal cycles did not contribute to verification scores. At the 14-20
95 day timescale around western Europe, the greatest skill was found in the boreal winter (austral
96 summer) months of December, January and February.

97 Pinson and Hagedorn (2012) and Lynch et al. (2014) restricted their verification studies to wind
98 speeds, but wind directions are also crucial to diagnosing whether land sea breezes - and the diurnal
99 wind cycle more generally - are being forecast correctly. Furthermore, no previous published
100 work has proposed a verification methodology to assess the accuracy of the diurnal wind cycle
101 in forecasts, or of the contributions made to this accuracy by human forecaster edits of model
102 output. Finally, no previously published work has considered the performance of ACCESS near
103 surface winds, which together with ECMWF, are the model guidance products most widely used

104 by Australian forecasters. Thus, the present study has two goals. First, to describe a methodology
105 for comparing human edited forecasts of the land-sea breeze to unedited model guidance forecasts,
106 in order to assess where and when human edits are producing an increase in accuracy. Second,
107 to apply this methodology across Australia. The remainder of this paper is organised as follows.
108 Section 2 describes the methodology in detail, section 3 provides results, and sections 4 and 5
109 provide a discussion and a conclusion, respectively.

110 **2. Data and Methods**

111 This study compares both edited and non-edited Australian Bureau of Meteorology forecast
112 data with automatic weather station (AWS) data across Australia. The comparison is performed
113 by first isolating the diurnal signals of each dataset, then comparing these signals on an hour-by-
114 hour basis. If the diurnal cycle cannot be resolved correctly using wind perturbations, it cannot be
115 resolved correctly in the overall wind fields, which are subject to additional synoptic scale errors
116 between the models and observations.

117 *a. Data*

118 Four datasets are considered in this study; they are the Australian Bureau of Meteorology's Of-
119 ficial wind forecast data, model data from the European Center for Medium Range Weather Fore-
120 casting (ECMWF), model data from the Australian Community Climate and Earth System Simu-
121 lator (ACCESS), and observational data from automatic weather stations. The Official, ECMWF
122 and ACCESS data are at a ?, ? degree spatial resolution respectively. What are the resolutions of
123 these datasets as they're used in Jive? Does the ACCESS model data in Jive Official, ACCESS
124 and AWS data exists at each UTC hour. ECMWF data exists at a three hour resolution. To be con-
125 sistent with the other data sets, ECMWF is therefore linearly interpolated to an hourly resolution:

126 this is also what happens in practice when forecasters load ECMWF wind data into the GFE. Both
127 ACCESS and ECMWF use parametrisation schemes to simulate sub-grid scale boundary layer
128 mixing and turbulence. ACCESS uses the schemes of Lock et al. (2000) and Louis (1979) for
129 unstable and stable boundary layers respectively (Bureau of Meteorology 2010). ECMWF uses
130 similar schemes that they develop in-house (European Center for Medium Range Weather Fore-
131 casting 2018). Data covers the austral winter months of June, July and August 2018; this short
132 time period was chosen to reduce the effect of changing seasonal and climatic conditions, changing
133 forecasting practice and staff, and of developments to the ACCESS and ECMWF models.

134 How is model/forecast data made consistent with AWS data in Jive - particularly regarding
135 heights? Are all stations 10 m above surface? Are all model/forecast data provided at the same
136 height?

137 Only station data from the seven Australian capital city airport automatic weather stations are
138 considered; Official, ECMWF and ACCESS data is (linearly?) interpolated to the coordinates
139 of the airport weather stations. Capital city airports have been chosen as the focus of this study
140 for a number of reasons. Automatic weather stations located at airports tend to provide the most
141 accurate wind data, and wind forecasts at airports are important to the aviation industry. Moreover,
142 the capital city airports are all reasonably close to coastlines, resulting in a clear diurnal signal.
143 Finally, these airports are also all close to their respective capital cities, which are high priority
144 regions for accurate forecasting. The datasets are hosted on the Bureau's Jive database, but are not
145 currently generally available, although the long term plan is for this to change. Can I extract and
146 host the data I need myself? Can I obtain copies of the relevant Jive Functions so that I can post
147 complete code online?

148 As described above, the Australian Bureau of Meteorology's official wind forecast is constructed
149 out of model data, which is then edited by human forecasters using the Graphical Forecast Editor

150 (GFE) software package. Australian forecasters typically construct wind forecasts out of model
151 data either from the European Center for Medium Range Weather Forecasting (ECMWF), or the
152 Australian Community Climate and Earth System Simulator (ACCESS). Testing whether the of-
153 ficial forecast data conforms more closely to the AWS observations than ECMWF or ACCESS
154 therefore provides a way to assess the extra accuracy gained by forecaster edits.

155 *b. Assessing Diurnal Cycles*

156 Although close to coastlines the land-sea breeze is generally the dominant diurnal wind process,
157 the overall diurnal signal may also include mountain-valley breezes, boundary layer mixing pro-
158 cesses, atmospheric tides, and urban heat island circulations. Forecasters typically edit model out-
159 put to account for *both* unresolved sea-breezes *and* unresolved boundary layer mixing; attempting
160 to focus solely on sea-breezes without examining the entire diurnal cycle therefore risks erroneous
161 conclusions, with the effects of one category of edit mistaken for another. In general it is hard to
162 separate boundary layer mixing edits from sea-breeze edits in the diurnal cycle composites, so this
163 point maybe needs to be reworked. Or could simply comment on this in the discussion.

164 Sea-breezes are therefore analysed by examining the overall diurnal signal in each dataset, with
165 the assumption that close to coastlines the land-sea breeze is the dominant diurnal process. The di-
166 urnal signal is identified by subtracting a twenty hour centred running mean *background wind* from
167 each zonal and meridional hourly wind data point. This provides a collection of zonal and merid-
168 ional wind *perturbation* datasets. Note that thinking of land-sea breezes in terms of perturbations
169 from a background wind may require a conceptual shift from the usual operational definitions.
170 A forecaster would likely define a sea-breeze to be a reversal in wind direction from a primar-
171 ily offshore flow during the night and morning, to an onshore flow in the afternoon and evening.

172 However, even if the wind is offshore the entire day, sea-breeze *perturbations* are generally still
 173 detectable as a weakening of the offshore flow throughout the afternoon and evening.

174 Note that subtracting background winds may raise concerns, because perturbations obviously
 175 depend on background winds. However, the forecaster does not have knowledge of the observa-
 176 tions when they make the diurnal process edits. They are implicitly assuming that the true mean
 177 state will be close enough to the predicted mean state - however this prediction is produced - to
 178 justify making diurnal edits on the basis of the predicted mean state.

179 Once the wind perturbation datasets have been constructed, the accuracy of the Official, AC-
 180 CESS and ECMWF diurnal cycles are quantified by first calculating the Euclidean distances of
 181 the perturbations at each hour from the corresponding AWS perturbations. For instance, to quan-
 182 tify how closely the Official forecast perturbations match the AWS observations, we calculate the
 183 Euclidean distances $|\mathbf{u}_{\text{AWS}} - \mathbf{u}_{\text{O}}|$ at each time step. The accuracy with which the Official and AC-
 184 CESS datasets resolve the diurnal cycle can then be compared by defining the *Wind Perturbation*
 185 *Index* (WPI)

$$\text{WPI}_{\text{OA}} \equiv |\mathbf{u}_{\text{AWS}} - \mathbf{u}_{\text{A}}| - |\mathbf{u}_{\text{AWS}} - \mathbf{u}_{\text{O}}|. \quad (1)$$

186 At a given time, the Official forecast wind perturbation is closer to the AWS perturbation than that
 187 of ACCESS if and only if $\text{WPI} > 0$. Similarly, the WPI can be used to provide a comparison of the
 188 Official and ECMWF datasets, or a comparison of the two model guidance datasets ACCESS and
 189 ECMWF.

190 To assess which dataset provides, in general, the most accurate representation of the diurnal cy-
 191 cle, we then take means of the WPI on an hourly basis; i.e. all the 00:00 UTC WPI values are
 192 averaged, all the 01:00 UTC values are averaged, and so forth. The sampling distributions of
 193 these means can then be modelled as Student's t -distributions, and from this we can calculate the
 194 probability that $\overline{\text{WPI}} > 0$ at each hour, where the bar denotes a temporal average. Temporal au-

195 tocorrelations of WPI, i.e. correlations between WPI values at a particular hour from one day to
 196 the next, are accounted for using the standard method of reducing the “effective” sample size to
 197 $n(1 - \rho_1) / (1 + \rho_1)$, where n is the actual sample size and ρ_1 is the lag-1 autocorrelation (Zwiers
 198 and von Storch 1995; Wilks 2011), although in practice temporal autocorrelations of WPI are ei-
 199 ther non-existent or very small. To assess how well the diurnal perturbations of an overall region
 200 are predicted, for instance those of the Victorian coastal station group (see Fig. ??), the perturba-
 201 tions across each station group are averaged before WPI values calculated. The temporal means
 202 and sampling distributions of the WPI are then calculated as before, with each value of WPI cal-
 203 culated from the spatially averaged perturbations treated as a single observation. This provides a
 204 conservative method for dealing with spatial correlation in the perturbations.

205 The advantage of the WPI method is it’s clarity and simplicity: we are essentially just comparing
 206 the magnitudes of vector differences, then applying a two sided t -test to determine whether one
 207 dataset’s perturbations are consistently closer to observations than another’s. One factor that com-
 208 plicates interpretation of statistics of WPI, is that the near surface winds observed in AWS data are
 209 consistently noisier than those of the Official, ECMWF and ACCESS forecasts. This is likely due
 210 to unresolved subgrid scale turbulence in the Official, ECMWF and ACCESS model datasets. It
 211 would be unreasonable to expect forecasters to be able to predict this essentially random additional
 212 observed variability, and so a direct comparison of observed and modelled diurnal cycles is overly
 213 stringent.

214 To reduce the significance of unpredictable noise, we also compare temporal averages of the
 215 perturbations for each dataset. These comparisons have less operational significance: people gen-
 216 erally care how well the actual weather forecast performed, not whether the average of a predicted
 217 quantity matched the average of an observed quantity. However, comparisons of averages arguably
 218 better represent what we can realistically expect from human forecaster edits, and from weather

forecasts overall, particularly in regards to small scale processes like sea-breezes. Furthermore, when temporal averages of perturbations are considered, the diurnal signal becomes dramatically clearer, and structural differences become much easier to diagnose.

To quantify how closely the temporally averaged Official forecast perturbations match those of the AWS observations, we calculate $|\bar{u}_{\text{AWS}} - \bar{u}_{\text{O}}|$ for each hour. To assess the performance of the Official temporally averaged perturbations against those ACCESS, we define the *Climatological Wind Perturbation Index* (CWPI)

$$\text{CWPI}_{\text{OA}} \equiv |\bar{u}_{\text{AWS}} - \bar{u}_{\text{O}}| - |\bar{u}_{\text{AWS}} - \bar{u}_{\text{A}}|. \quad (2)$$

As with the WPI, the CWPI can also be used to provide a comparison of the Official and ECMWF datasets, or a comparison of the two model guidance datasets ACCESS and ECMWF. Uncertainty in the CWPI is estimated through bootstrapping (Efron 1979). This is done by performing resampling with replacement on the underlying perturbation datasets, and calculating the CWPI multiple times using these resampled datasets. This provides a distribution of CWPI values, from which the probability that $\text{CWPI} > 0$ can be calculated. Similarly to with the WPI, performance over a particular region can be assessed by first averaging perturbation values over multiple stations before the CWPI is calculated.

Although the WPI and CWPI provide quantitative information on the accuracy of the diurnal cycle at different times of day, they do not provide much information about the structure of the diurnal wind cycles of each dataset, or provide insight into the reason one dataset is outperforming another. Gille et al. (2005) obtained summary statistics on the observed structure of temporally averaged diurnal wind cycles across the globe by using linear regression to calculate the coefficients u_i, v_i

239 $i = 0, 1, 2$, for the elliptical fit

$$u = u_0 + u_1 \cos(\omega t) + u_2 \sin(\omega t), \quad (3)$$

$$v = v_0 + v_1 \sin(\omega t) + v_2 \sin(\omega t), \quad (4)$$

240 where ω is the angular frequency of the earth and t is the local solar time in seconds. Descriptive
 241 quantities - like the angle the semimajor axis of the ellipse makes with the horizontal - were then
 242 calculated directly from the coefficients u_1 , u_2 , v_1 and v_2 .

243 Gille et al. (2005) applied this fit to satellite scatterometer wind observations, which after tem-
 244 poral averaging provided only four temporal datapoints at each $0.25^\circ \times 0.25^\circ$ spatial grid cell. As
 245 such, their fit was very good, explaining over 90% of the wind variability in each spatial gridcell.
 246 However, the choice of ellipse parametrisation in equations 5 and 6 assumes that datapoints lie on
 247 the ellipse at equal intervals of time t . When observational or model data with an hourly or smaller
 248 timestep is considered, this assumption becomes too stringent, as heating asymmetries imply that
 249 wind perturbations evolve much more rapidly during the day than at night (see Fig. XX). **Note**
 250 **I'm also basing this point on knowledge of the land vs sea breeze, and knowledge of heating vs**
 251 **cooling asymmetries (Brown et al. 2017, e.g.).**

252 Thus, we model the climatological diurnal cycles with the equations

$$u = u_0 + u_1 \cos(\alpha(\psi, t)) + u_2 \sin(\alpha(\psi, t)), \quad (5)$$

$$v = v_0 + v_1 \sin(\alpha(\psi, t)) + v_2 \sin(\alpha(\psi, t)), \quad (6)$$

253 with α the function from $[0, 24) \times [0, 2\pi) \rightarrow [0, 2\pi)$ given by

$$\alpha(\psi, t) \equiv \pi \left[\sin \left(\pi \frac{(t - \psi) \bmod 24}{24} - \frac{\pi}{2} \right) + 1 \right], \quad (7)$$

where t is time in units of hours UTC, and ψ gives to the time when the wind perturbations vary least with time. **Need to confirm whether least or most!** For each climatological diurnal wind cycle, we solve for the seven parameters $u_0, u_1, u_2, v_0, v_1, v_2$ and ψ using nonlinear regression.

Descriptive quantities can then be calculated from these parameters. The value of α at which the winds align with the semimajor axis, α_M , satisfies

$$\alpha_M = \frac{1}{2} \arctan \left(\frac{2(u_1 u_2 + v_1 v_2)}{u_1^2 + v_1^2 - u_2^2 - v_2^2} \right) \bmod \pi, \quad (8)$$

The time at which the perturbations align with the major axis t_M can then be calculated by inverting equation (7), fixing ψ to the value obtained from the nonlinear regression. The lengths of the semimajor and semiminor axes, and the angle the semimajor axis makes with lines of latitude ϕ , can then be calculated from α_M using the same expressions as Gille et al. (2005).

3. Results

In this section, the methods described in section ?? are applied to Australian forecast and station data over the months of June, July and August (austral winter) 2018. First, error is assessed on a daily basis using the Wind Perturbation Index (WPI) at three different spatial scales. Second, overall seasonal biases during this time period are assessed using the Climatological Wind Perturbation Index CWPI, and by comparing quantities derived from ellipses fitted to the climatological wind perturbations. Unless otherwise stated, values throughout this section are provided to two significant figures.

a. Daily Comparison

Figure 2 provides the mean wind perturbation index values $\overline{\text{wpi}}$ and confidence scores $P(\overline{\text{WPI}} > 0)$ for the coastal station groups for $\overline{\text{wpi}}_{\text{OA}}$, $\overline{\text{wpi}}_{\text{OE}}$ and $\overline{\text{wpi}}_{\text{EA}}$, which represent the the Official versus ACCESS, Official versus ECMWF, and ECMWF versus ACCESS comparisons,

275 respectively. Values of \overline{wpi}_{OA} and \overline{wpi}_{OE} are negative for the majority of station groups and hours,
 276 and often both $P(\overline{WPI}_{OA} > 0) < 5\%$ and $P(\overline{WPI}_{OE} > 0) < 5\%$. This implies that at this level of
 277 spatial aggregation, there is often high confidence that both the unedited ACCESS and ECMWF
 278 models outperform the Official forecast. The lowest \overline{wpi} values of -0.9 kn occur for the NT sta-
 279 tion group at 23:00 and 00:00 UTC for both \overline{wpi}_{OA} and \overline{wpi}_{OE} , with $\overline{wpi}_{EA} = 0$ kn. Comparatively
 280 low values also occur at 08:00 UTC with $\overline{wpi}_{OA} = \overline{wpi}_{OE} = -0.6$ kn, but $\overline{wpi}_{EA} = 0$ kn. This
 281 suggests the Official forecast may be performing particularly poorly over the NT station group.

282 Although Official outperforms at least one of ACCESS or ECMWF with high confidence at
 283 a few dozen times and station groups, there is only one group and time where it outperforms
 284 both. At 05:00 UTC over the South WA station group, $\overline{wpi}_{OA} = 0.2$ kn and $\overline{wpi}_{OE} = 0.1$ kn, both
 285 with confidence scores $\geq 95\%$, although the actual \overline{wpi} values are comparatively small. Note that
 286 ECMWF generally outperforms ACCESS from 10:00 - 14:00 UTC, with the South WA station
 287 group being the main exception.

288 Using the NT and South WA station groups as case studies, Figures 3 a) and b) provide time
 289 series of wpi_{OA} and wpi_{OE} for, a), the NT station group at 23:00 UTC, and b), the South WA
 290 station group at 05:00 UTC. The wpi_{OA} and wpi_{OE} values for the NT station group show significant
 291 temporal variability over the three month period, exceeding -2 kn on at least 10 days each, and
 292 occasionally becoming positive. The wpi values for the South WA station at 05:00 UTC also show
 293 significant temporal variability, with wpi_{OA} and wpi_{OE} each exceeding 1 kn on at least 9 separate
 294 days, despite \overline{wpi}_{OA} and \overline{wpi}_{OE} being small.

295 Fig. 3 a) shows that there are four days where wpi_{OA} and wpi_{OE} are both less than -2 kn: the
 296 8th of June and the 3rd, 9th and 10th of July. Figures 3 c) and d) show hodographs of the winds
 297 and wind perturbations, respectively, at each hour UTC for the AWS observations, Official fore-
 298 cast, and ACCESS and ECMWF model datasets on the 3rd of July, which provides an interest-

ing example. Figure 3 e) shows that the Official wind forecast on this day was likely based on edited ACCESS from 00:00 to 06:00 UTC, then edited ECMWF from 07:00 to 13:00 UTC, then unedited ACCESS from 15:00 to 21:00 UTC. The final two hours of the forecast show the Official winds acquiring a stronger east-northeasterly component than either the AWS observations, ACCESS, or ECMWF; this rapid, exaggerated change is even clearer in the perturbation hodograph shown in Fig. 3 f). Note that at this time of year the prevailing winds throughout the NT are east-southeasterly, and 22:00 UTC corresponds to $\approx 08:30$ LST in this region, so the rapid departure of the Official forecast from ACCESS at this time likely represents an edit made by a forecaster to capture boundary layer mixing processes. Figure 4 a) shows the first ten values from wind soundings at Darwin Airport - the nearest station to issue vertical wind soundings - at 12:00 UTC on July 3rd and 00:00 UTC on July 4th. In both instances the winds are indeed east-southeasterly, and so the rapidly changing wind perturbations at 22:00 UTC in the Official forecast likely reflect a boundary layer mixing edit that has been applied either too early, or has strengthened the southeasterly component of the winds too much. The 8th of June and 9th and 10th of July examples are all similar in this respect.

Considering now the South WA station group, Fig. 3 b) shows that wpi_{OA} and wpi_{OE} both exceed 1 kn on the 9th of June and the 3rd of August. Figures 3 c) and d) show hodographs of the winds and wind perturbations, respectively, at each hour UTC for the AWS observations, Official forecast, and ACCESS and ECMWF model datasets on the 9th of June, which is the more interesting example. The perturbation hodograph shows both ECMWF and ACCESS underpredicting the amplitude of the diurnal wind cycle on this day. In each dataset the 05:00 UTC perturbations are westerly to northwesterly, and given the orientation of the South WA coastline (see Fig. 1) and the fact that 05:00 UTC corresponds to $\approx 13:00$ local solar time (LST) in this region, the perturbations likely indicate boundary layer mixing processes, rather than the land-sea breeze. Furthermore, the

323 AWS perturbations rapidly become northwesterly between 01:00 and 02:00 UTC, \approx 09:00 - 10:00
324 LST, which would be about three hours after the sun has risen, consistent with a boundary layer
325 mixing mechanism.

326 Figure 4 provides hodographs of wind with height throughout the first two km of the atmosphere
327 between 12:00 UTC on the 8th June and 12:00 UTC on the 9th June; the soundings were taken at
328 Perth Airport, which is the nearest station to the South WA station group to provide wind sound-
329 ings. The 8th June 12:00 UTC hodograph shows surface northerlies of \approx 6 kn, becoming west to
330 northwesterlies of over 20 kn 2.4 km above the surface. A forecaster basing a model edit of the
331 following days winds on this sounding would therefore gradually strengthen the westerly compo-
332 nent of the surface winds in the hours after sunrise. However, the subsequent sounding at 00:00
333 UTC on the 9th of June shows that the winds acquire a strong northerly component of 30 kn in the
334 first 500 m of the atmosphere, with the final sounding indicating a strong northwesterly wind at
335 725 m persisting until 12:00 UTC. In Fig. 3 d), the Official perturbations from 04:00 to 07:00 UTC
336 show stronger westerly perturbations than either ACCESS or ECMWF, improving the amplitude
337 of Official's diurnal wind cycle. However, the AWS perturbations are more northerly than those of
338 Official, and so the Official forecast winds have been strengthened in a slightly incorrect direction.
339 An explanation for this discrepancy is that the Official forecast for the southwest region of WA has
340 been edited based on the June 8th 12:00 UTC Perth Airport sounding, with the winds above the
341 surface changing direction in the subsequent 12 hours. Note that the 3rd of August example is sim-
342 ilar, although in this case the Official forecast slightly improves both the magnitude and direction
343 of the 05:00 UTC wind perturbations.

344 Figure 5 presents the \overline{wpi} values and confidence scores for the Official versus ECMWF com-
345 parisons, i.e. \overline{wpi}_{OE} and $P(\overline{WPI}_{OE} > 0)$, for the airport stations, and airport station groups. The
346 results for the airport stations are noisier than the analogous results for the coastal station groups

in Figures 2 c) and d), although they do share some similarities. Official outperforms ECMWF at 01:00 and 02:00 UTC at both the Darwin airport station and the NT station group, although ECMWF outperforms Official between 08:00 and 14:00 UTC at Darwin and Brisbane airports, and the corresponding NT and QLD station groups, with the exception of the QLD station group at 12:00 UTC where $\overline{wpi}_{OE} = 0$. ECMWF also outperforms Official at Hobart airport at almost all hours of the day, and at Adelaide and Canberra airports from 11:00 to 14:00 UTC.

For the remaining stations and times, only the Perth airport station at 06:00 UTC and the Melbourne airport station at 01:00 UTC exhibit $\overline{wpi}_{OE} > 0$ with $P(\overline{WPI}_{OE} > 0) \geq 95\%$. However, in both cases $\overline{wpi}_{OE} = 0.3$, which is small compared to the maximum value of 1.0 which occurs at the Darwin airport station at 02:00 UTC. Furthermore, in both cases there is no clear pattern to the \overline{wpi}_{OE} values over the rest of the day. Given the random appearance of the \overline{wpi}_{OE} values, the *multiplicity problem* (Wilks 2011, p. 178) requires care be taken before giving meaning to these two examples: i.e., given that we are calculating twenty four confidence scores for eight stations, then assuming WPI were uncorrelated across each station and hour we would expect to find $0.05 \times 24 \times 8 \approx 10$ instances where $P(\overline{WPI}_{OE} > 0) \geq 95\%$, even if \overline{WPI}_{OE} was in fact equal to zero. **Comment on performance versus ACCESS.**

For the airport station groups, ECMWF outperforms Official for the majority of station groups and times. The main exception is the Darwin airport station group, where Official outperforms ECMWF at 02:00 UTC, and there is ambiguity as to whether Official or ECMWF performs better at 01:00, 03:00 and 04:00 UTC, and from 15:00 to 22:00 UTC. In the analogous comparisons of Official and ACCESS (not shown), the airport station results are similarly noisy, although the airport station group results are slightly more favourable to Official, with Official outperforming ACCESS from 10:00 to 12:00 UTC at the Brisbane station group, and fewer occasions overall where ACCESS outperforms Official than ECMWF does.

Figure 5 shows the $\overline{\text{wpi}}$ values and confidence scores for the ECMWF versus ACCESS comparisons, i.e. $\overline{\text{wpi}}_{\text{EA}}$ and $P(\overline{\text{WPI}}_{\text{EA}} > 0)$, for the airport stations, and airport station groups. As with the Official versus ECMWF comparison in Fig. 5, the results for the airport stations are noisy, but more often than not show that ECMWF outperforms ACCESS. The results for the airport station group show ECMWF usually outperforms ACCESS, the main exceptions being the Darwin and Canberra airport station groups.

At face value, the fact that ECMWF generally outperforms ACCESS at these scales is surprising, as ACCESS runs at a higher spatiotemporal resolution than ECMWF, and is calibrated for Australian conditions, so one would expect ACCESS would better resolve small scale processes like the land-sea breeze and boundary layer mixing processes. However, these results are unsurprising if one considers the scales at which predictable atmospheric motion occurs, and the scales being resolved by AWS, ACCESS and ECMWF. The AWS data resolves motion with time scales as low as 10 minutes, and arbitrarily small spatial scales: it therefore includes highly unpredictable eddy turbulence. This explains why the results for the airport stations are noisier than for the airport station groups or coastal station groups. Furthermore, because ACCESS runs at a higher resolution than ECMWF, it includes additional scales of motion, and therefore adds additional variability to the wind fields. Unless this additional variability in ACCESS is perfectly correlated with observations, the average of $|\mathbf{u}_{\text{AWS}} - \mathbf{u}_{\text{A}}|$ will therefore increase, unless this additional variability is compensated for by a reduction in bias, i.e. $|\overline{\mathbf{u}}_{\text{AWS}} - \overline{\mathbf{u}}_{\text{A}}|$ decreases. These ideas are discussed in greater detail in section 4. Note finally that the results for the Official versus ECMWF comparison in Fig. 5 largely mirror those of the ECMWF versus ACCESS comparison in Fig. 5, e.g. for the Darwin airport station and station group, Official outperforms ECMWF at the same times that ACCESS does, suggesting that either the Official forecast at these spatial scales is largely based on ACCESS, or that ECMWF is highly biased at these scales and times.

b. Seasonal Comparison

Figure 5 provides the climatological wind perturbation index values, $cwpi$, and confidence scores, $P(CWPI > 0)$, for the coastal station groups for $cwpi_{OA}$, $cwpi_{OE}$ and $cwpi_{EA}$, which represent the Official versus ACCESS, Official versus ECMWF, and ECMWF versus ACCESS comparisons, respectively. At the NT station group Official outperforms both ACCESS and ECMWF at 03:00 UTC with $cwpi_{OA} = cwpi_{OE} = 0.4$, $P(cwpi_{OA} > 0) = 94\%$ and $P(cwpi_{OE} > 0) = 93\%$. However, both ACCESS and ECMWF outperform Official at 23:00 and 00:00 UTC, consistent with the \overline{wpi} results in Fig. 2. The NT station group results are discussed in more detail in section 4.

At the North WA station group at 01:00, 03:00 and 04:00, Official outperforms ACCESS with confidence scores of 77, 78 and 90%, respectively; Official also outperforms ECMWF at 01:00 and 02:00 UTC with confidence scores above 99%. Figure 6 a) shows that ECMWF's poor performance at 01:00 and 02:00 UTC is simply due to its linear interpolation at these times, whereas Official's outperformance of ACCESS at 01:00, 03:00 and 04:00 is due to ACCESS's climatological diurnal cycle being slightly out of phase with that of the AWS observations, and the Official forecast appearing to correct for this somewhat. Both Official and ECMWF slightly exaggerate the magnitude of the climatological sea-breeze with ACCESS doing a good job in this regard.

At the South WA station group from 01:00 to 05:00 UTC, $cwpi_{OE}$ is positive with confidence scores of at least 88%, although $cwpi_{OA}$ is negative or zero at these times. Figure 6 b) shows that ECMWF underestimates the westerly perturbations at these times, with these perturbations likely associated with boundary layer mixing processes, as discussed in section a. Each of Official, ACCESS and ECMWF underestimate the amplitude of the diurnal cycle between 02:00 and 10:00 UTC, including both the westerly perturbations and the southerly sea-breeze perturbations.

418 At the NSW station group from 17:00 to 19:00 UTC, $cwpi_{OA}$ and $cwpi_{OE}$ are at least 0.4 and 0.1
419 kn, respectively, with confidence scores of at least 95% and 75%, respectively. Figure 6 c) shows
420 that these times correspond to a strange “dimple” in perturbation hodograph that is present in all
421 four datasets. The Official hodograph closely resembles that of ACCESS, except for this dimple,
422 which has been exaggerated relative to ACCESS. Don’t know what is going on here. Figure 6 c)
423 also shows that although ECMWF exaggerates the amplitude of the easterly sea-breeze perturba-
424 tions, it captures the narrower shape of the AWS hodograph better than Official or ACCESS.

425 At the SA station group from 01:00 to 05:00 UTC and 09:00 to 11:00 UTC both $cwpi_{OA}$ and
426 $cwpi_{OE}$ are positive, with maximum values of 0.4 and 0.1 kn, although confidence scores do not
427 exceed 88% and 65% respectively. Figure 6 shows that the Official forecast captures the amplitude
428 of the perturbations from 01:00 to 05:00 UTC almost perfectly, matching the amplitude of the
429 AWS perturbations better than both ACCESS and ECMWF. However, the Official diurnal cycle is
430 slightly out of phase with the AWS cycle during this period, explaining why Official only slightly
431 outperforms ACCESS in the results of Figures 5 a) and b).

432 While the $cwpi$ values and confidence scores of Fig. 5 provide detailed information on which
433 dataset’s climatological diurnal cycle best matches those of the AWS observations, $cwpi$ on it’s
434 own reveals little about the structure of the diurnal cycle, and provides little insight into forecast
435 accuracy could be improved. Note that the hodographs in Fig. 6 are roughly elliptical in shape,
436 suggesting that descriptive quantities can be estimated by fitting equations (5) and (6) to the zonal
437 and meridional climatological perturbations, then calculating these quantities from the fit, as de-
438 scribed in section 2.

439 Figure 8 provides the R^2 values for the fits of the zonal and meridional perturbations to equations
440 (5) and (6), respectively. The fit performs best at the coastal station group spatial scale, with
441 R^2 generally above 95%. It also performs well at the airport station and airport station group

scales, with a few exceptions, including the ACCESS and Official meridional perturbations at the Canberra airport station group, and the ECMWF zonal perturbations at Melbourne airport.

The ellipse fits are used to derive four descriptive quantities: amplitude (half the length of the semi-major axis), eccentricity, orientation (the angle the semi-major axis makes with lines of latitude) and the time of the peak in the diurnal cycle (the time at which the perturbations align with the semi-major axis, ignoring translational coefficients). Figure 9 provides these four quantities for each dataset and location across the three spatial scales. A variety of structural differences are apparent at a number of locations and scales. For example, Fig. 9 a) shows that at Brisbane airport, the amplitude of the AWS diurnal cycle is at least 1 kn greater than Official, ACCESS and ECMWF, and Fig. 9 c) shows that the orientation of the AWS diurnal cycle hodograph is at least 20 degrees (anti-clockwise) from the other datasets. Figures 10 a) and b) show hodographs of the Brisbane airport perturbation climatology and ellipse fit, respectively. Although the ellipse fit suppresses some of the asymmetric details, it captures the amplitudes and orientations of the real climatological diurnal cycles well. In this case the results show that the average AWS sea-breeze approaches from the northeast, whereas the forecast and model sea-breezes approach more from the east-northeast. To check whether this just represents a direction bias of the Brisbane Airport station, Fig. 9 shows the climatological perturbations at the nearby Spitfire Channel station (see Fig. ?? for the location of this station, and other stations referred to in this section). While the amplitude bias is smaller at Spitfire Channel than Brisbane Airport, the directional bias is at least as high; a similar directional bias is evident at the nearby Inner Beacon station, although the bias is smaller than at Spitfire Channel and Brisbane Airport. Thus, the directional bias in Official, ACCESS and ECMWF at these stations is likely genuine, and not just a consequence of biased AWS observations. Figure 1 x) shows there are two small islands to the east of Brisbane airport; the more northwesterly orientation of the Brisbane Airport sea-breeze suggests these islands may

466 be channelling winds between the east coast of Brisbane and the west coasts of these islands, and
467 that this local effect is not being captured in Official, ACCESS or ECMWF.

468 Another example is the Hobart Airport station. Figure 9 c) shows that the ellipse fits for the
469 AWS perturbations are oriented 31, 35 and 62 degrees anti-clockwise from the ECMWF, Official
470 and ACCESS ellipse fits, respectively. Figures 8 a) and b) show that the ellipse fit for the AWS
471 perturbations at Hobart airport only achieve R^2 values of 59% and 68% for the u and v compo-
472 nents, respectively, although figures 10 d) and e) show that the fit still captures the orientation
473 accurately; the deficiency is more with the amplitude of the AWS diurnal cycle. Figure 8 c) shows
474 the climatological perturbations at the Hobart (city) station, which also show a large difference
475 in orientation between ACCESS and AWS. Given the timing of the westerly perturbations in AC-
476 CESS, and the fact that the prevailing winds around Tasmania are Hobart, these results suggest
477 that ACCESS is exaggerating the boundary layer mixing processes involved in the diurnal cycle,
478 whereas ECMWF better captures the southerly sea-breeze component of the cycle.

479 The South WA station group also provides an interesting example. Here the ACCESS and
480 Official ellipse fits are oriented at least 49 degrees anti-clockwise from those of AWS and ECMWF,
481 and the time of the peak in the diurnal cycles of ACCESS and Official is at least 4.3 hours earlier
482 than AWS and ECMWF. This occurs because eccentricity values are low for this station group,
483 and Figure 6 b) shows that the westerly perturbations associated with boundary layer mixing are
484 slightly faster than the corresponding southerly sea-breeze perturbations, which peak later, for
485 both ACCESS and Official, but slightly slower for ECMWF and Official. A similar issue affects
486 the VIC station group, explaining why the AWS ellipse fit is oriented at least 49 degrees anti-
487 clockwise from those of the other datasets.

488 Finally, figure 9 suggests that at the Darwin Airport, Darwin Airport station group, and NT sta-
489 tion group, the AWS wind perturbations align with the semi-major axis after those of the other

490 datasets, and in the case of the NT station group alignment occurs at least 2.3 hours later; fur-
 491 thermore, the amplitude of the Official ellipse fit is in each case higher than those of the other
 492 datasets. “Alignment” is probably the wrong word here. Figure 11 shows that these biases are
 493 indeed evident in the perturbation climatologies themselves, with the exception of the Darwin
 494 Airport amplitude bias, where the asymmetric hodograph shapes lead to the ellipse fit underesti-
 495 mating the amplitude of the AWS diurnal cycle Needs to be clarified to better distinguish between
 496 “ellipse” amplitude and diurnal cycle amplitude. Furthermore, should we interpret the NT station
 497 group results as genuine evidence of a timing bias?

498 4. Discussion

499 The two most important results of section 3 to explain are, first, why equations 5 and 6 provide
 500 such a good fit to the climatological perturbations and, second, why there are such substantial
 501 changes in the performance of the Official forecast at the different spatial and temporal scales.

502 The idea that diurnal wind cycles can be described by ellipses originated with Haurwitz (1947).
 503 Haurwitz obtained exact solutions for u and v resembling equations (3) and (4) for the simple
 504 model

$$\frac{du}{dt} - fv + ku = F_x - F(t) \quad (9)$$

$$\frac{dv}{dt} + fu + kv = F_y \quad (10)$$

505 where u, v are taken in a coordinate system where the u axis is normal to the coast, f is the Coriolis
 506 parameter, k is a linear friction coefficient, (F_x, F_y) represents a constant synoptic scale pressure
 507 gradient force, ω is the angular frequency of earth’s rotation, and

$$F(t) = \frac{A}{\pi} + \frac{A}{2} \cos(\omega t) \quad (11)$$

is the pressure gradient force normal to the coastline induced by the diurnally varying air temperature contrast over the land and sea surfaces. Kusuda and Alpert (1983) extended this model slightly, but the fundamentals are the same. The limitations of this model are discussed extensively by Haurwitz (1947) and Kusuda and Alpert (1983), but the most important given the results of section 3 involve the choice of $F(t)$, which does not sufficiently capture the asymmetries in daytime heating and nighttime cooling, and the fact that the model has no vertical dimension, and therefore cannot capture the boundary layer mixing processes that in many cases play a significant role in the diurnal wind cycle. This might work better in the introduction or methods sections - there's not actually very much to discuss!

I tried modifying the pressure perturbation terms $\frac{A}{\pi} + \frac{A}{2} \cos(\omega t)$ so that the new ellipse fit of equations (5) and (6) become solutions to equations (9) and (10), but with no luck. For example, simply changing to $F(t)$ to $\frac{A}{\pi} + \frac{A}{2} \cos(\alpha(\psi, t))$ doesn't work, nor does expanding this expression as a Fourier series and solving each term individually.

The second result of section 3 that requires explanation are the differences in the performance of the Official forecast at the different spatial and temporal scales. Consider first just the zonal components of the AWS and Official wind perturbations, denoted by u_{AWS} and u_{O} respectively. Considering just the values at a particular hour UTC, at a particular station, over the entire June, July, August time period, the mean square error $\text{mse}(u_{\text{AWS}}, u_{\text{O}}) = \overline{(u_{\text{AWS}} - u_{\text{O}})^2}$ can be decomposed

$$\text{mse}(u_{\text{AWS}}, u_{\text{O}}) = \underbrace{\text{var}(u_{\text{AWS}}) + \text{var}(u_{\text{O}}) - 2 \cdot \text{covar}(u_{\text{AWS}}, u_{\text{O}})}_{\text{var}(u_{\text{AWS}} - u_{\text{O}})} + \underbrace{(\bar{u}_{\text{AWS}} - \bar{u}_{\text{O}})^2}_{\text{bias}^2} \quad (12)$$

where var, covar and over-bars denote the sample variance, covariance and mean respectively. The first three terms are the total variance of $u_{\text{AWS}} - u_{\text{O}}$, whereas the last term is the square of the bias between u_{AWS} and u_{O} . This decomposition can also be applied to wind perturbations that have first

530 been spatially averaged over a station group, and to $\text{mse}(u_{\text{AWS}}, u_{\text{E}})$ and $\text{mse}(u_{\text{AWS}}, u_{\text{A}})$, where u_{E}
531 and u_{A} are the ECMWF and ACCESS zonal perturbations, respectively.

532 Figure 12 shows each term in the mean square error decomposition of equation 12 for both
533 $\text{mse}(u_{\text{AWS}}, u_{\text{O}})$ and $\text{mse}(u_{\text{AWS}}, u_{\text{E}})$, for Darwin Airport, the Darwin station group, and the NT sta-
534 tion group. At Darwin Airport, $\text{mse}(u_{\text{AWS}}, u_{\text{O}})$ exceeds $\text{mse}(u_{\text{AWS}}, u_{\text{E}})$ from 04:00 to 16:00 UTC
535 due to higher total variance, whereas outside of these times $\text{mse}(u_{\text{AWS}}, u_{\text{E}})$ exceeds $\text{mse}(u_{\text{AWS}}, u_{\text{O}})$
536 due to larger bias. The higher total variance of $u_{\text{AWS}} - u_{\text{O}}$ occurs because $\text{var}(u_{\text{O}}) > \text{var}(u_{\text{E}})$, with
537 this additional variability mostly random from 04:00 to 14:00 UTC, i.e. u_{O} is not sufficiently cor-
538 related with u_{AWS} at these times for the additional variability of u_{O} to produce a reduction in mean
539 square error. Thus, while the bias between Official and AWS is lower, or about the same, as that be-
540 tween ECMWF and AWS, the higher random variability of Official results in higher mean square
541 error for most of the day. Figure 13 shows similar conclusions can be drawn for the meridional
542 perturbations at Darwin Airport, although in this case $\text{var}(u_{\text{O}}) > \text{var}(u_{\text{E}})$ for the entire day. Most
543 of the difference between the WPI and CWPI scores for the Official versus ECMWF comparison
544 at Darwin Airport in Figures 5 and 7, respectively, can be explained through the different mean
545 square error and bias terms for the zonal perturbations alone. Figure 11 a) shows that ECMWF's
546 climatological perturbations underestimate the easterly perturbations from 00:00 to 03:00 UTC,
547 which are presumably associated with boundary layer mixing processes. Official does a better job
548 of resolving these easterly perturbations, but is generally outperformed by ECMWF in resolving
549 the northerly sea-breeze perturbations. Similar points can be made for the Darwin and NT coastal
550 station groups. While spatial averaging reduces a portion of the unpredictable variability in Offi-
551 cial, Official also often has larger meridional biases at these scales compared to ECMWF. Figures
552 11 and 9 show that these biases can be explained in terms of amplitude and orientation differences
553 between Official, ECMWF and AWS.

554 These examples illustrate the idea that the additional unpredictable variability introduced by a
555 higher resolution edited forecast needs to be “paid for” by a reduction in bias, otherwise the net re-
556 sult will just be an increase in error. However, although a high resolution edited forecast may have
557 higher mean squared error compared with observations than an unedited low resolution model, the
558 former may capture variability more realistically, and hence better represent the possibility of ex-
559 tremes, even if the timing of these extremes is unpredictable; which of the two constitutes a better
560 forecast therefore depends entirely on the application. For instance, in engineering applications,
561 the possibility of wind extremes of a certain magnitude may be most important, regardless of when
562 they occur, whereas in aviation or sailing it may be more important to minimise the mean square
563 error. This is obviously speculation as I know little about either of these applications. I hope there
564 are more appropriate examples. The fact that high and low resolution model guidance products are
565 used at different times, and on different days, implies that the Official forecast is inconsistent in
566 which measures of accuracy it intends to maximise, and more thought therefore needs to be given
567 to this issue.

568 5. Conclusion

569 We have

570 References

- 571 Brown, A. L., C. L. Vincent, T. P. Lane, E. Short, and H. Nguyen, 2017: Scatterometer estimates
572 of the tropical sea-breeze circulation near Darwin, with comparison to regional models. *Quart.*
573 *J. Roy. Meteor. Soc.*, doi:10.1002/qj.3131.
- 574 Bureau of Meteorology, 2010: Operational implementation of the ACCESS numerical weather
575 prediction systems. Tech. rep., Bureau of Meteorology, Melbourne, Victoria. [Available online

at <http://www.bom.gov.au/australia/charts/bulletins/apob83.pdf>].

Bureau of Meteorology, 2019: Meteye. Bureau of Meteorology, [\[http://www.bom.gov.au/australia/meteye/\]](http://www.bom.gov.au/australia/meteye/).

Ebert, E. E., 2008: Fuzzy verification of high-resolution gridded forecasts: a review and proposed framework. *Meteor. Appl.*, **15** (1), 51–64, doi:10.1002/met.25, URL <https://rmets.onlinelibrary.wiley.com/doi/abs/10.1002/met.25>, <https://rmets.onlinelibrary.wiley.com/doi/pdf/10.1002/met.25>.

Efron, B., 1979: Bootstrap methods: Another look at the jackknife. *The Annals of Statistics*, **7** (1), 1–26, doi:10.1214/aos/1176344552.

European Center for Medium Range Weather Forecasting, 2018: *Part IV : Physical processes*. No. 4, IFS Documentation, European Center for Medium Range Weather Forecasting, [Available online at <https://www.ecmwf.int/node/18714>].

Gille, S. T., S. G. Llewellyn Smith, and N. M. Statom, 2005: Global observations of the land breeze. *Geophysical Research Letters*, **32** (5), doi:10.1029/2004GL022139, URL <https://agupubs.onlinelibrary.wiley.com/doi/abs/10.1029/2004GL022139>.

Haurwitz, B., 1947: Comments on the sea-breeze circulation. *Journal of Meteorology*, **4** (1), 1–8, doi:10.1175/1520-0469(1947)004<0001:COTSBC>2.0.CO;2, URL [https://doi.org/10.1175/1520-0469\(1947\)004<0001:COTSBC>2.0.CO;2](https://doi.org/10.1175/1520-0469(1947)004<0001:COTSBC>2.0.CO;2), [https://doi.org/10.1175/1520-0469\(1947\)004<0001:COTSBC>2.0.CO;2](https://doi.org/10.1175/1520-0469(1947)004<0001:COTSBC>2.0.CO;2).

Kusuda, M., and P. Alpert, 1983: Anti-clockwise rotation of the wind hodograph. part i: Theoretical study. *Journal of the Atmospheric Sciences*, **40** (2), 487–499,

doi:10.1175/1520-0469(1983)040<0487:ACROTW>2.0.CO;2, URL [https://doi.org/10.1175/1520-0469\(1983\)040<0487:ACROTW>2.0.CO;2](https://doi.org/10.1175/1520-0469(1983)040<0487:ACROTW>2.0.CO;2).

Lee, X., 2018: *Fundamentals of boundary-layer meteorology*. Springer atmospheric sciences, Springer.

Lock, A. P., A. R. Brown, M. R. Bush, G. M. Martin, and R. N. B. Smith, 2000: A new boundary layer mixing scheme. part i: Scheme description and single-column model tests. *Monthly Weather Review*, **128** (9), 3187–3199, doi:10.1175/1520-0493(2000)128<3187:ANBLMS>2.0.CO;2, URL [https://doi.org/10.1175/1520-0493\(2000\)128<3187:ANBLMS>2.0.CO;2](https://doi.org/10.1175/1520-0493(2000)128<3187:ANBLMS>2.0.CO;2), [https://doi.org/10.1175/1520-0493\(2000\)128<3187:ANBLMS>2.0.CO;2](https://doi.org/10.1175/1520-0493(2000)128<3187:ANBLMS>2.0.CO;2).

Louis, J.-F., 1979: A parametric model of vertical eddy fluxes in the atmosphere. *Boundary-Layer Meteorology*, **17** (2), 187–202, doi:10.1007/BF00117978, URL <https://doi.org/10.1007/BF00117978>.

Lynch, K. J., D. J. Brayshaw, and A. Charlton-Perez, 2014: Verification of european sub-seasonal wind speed forecasts. *Monthly Weather Review*, **142** (8), 2978–2990, doi:10.1175/MWR-D-13-00341.1, URL <https://doi.org/10.1175/MWR-D-13-00341.1>, <https://doi.org/10.1175/MWR-D-13-00341.1>.

Pinson, P., and R. Hagedorn, 2012: Verification of the ecmwf ensemble forecasts of wind speed against analyses and observations. *Meteor. Appl.*, **19** (4), 484–500, doi:10.1002/met.283, URL <https://rmets.onlinelibrary.wiley.com/doi/abs/10.1002/met.283>, <https://rmets.onlinelibrary.wiley.com/doi/pdf/10.1002/met.283>.

Smith, J. C., R. Thresher, R. Zavadil, E. DeMeo, R. Piwko, B. Ernst, and T. Ackermann, 2009: A mighty wind. *IEEE Power and Energy Magazine*, **7** (2), 41–51, doi:10.1109/MPE.2008.931492.

619 Wilks, D. S., 2011: *Statistical methods in the atmospheric sciences. [electronic resource]*. Inter-
620 national geophysics series: v. 100, Elsevier.

621 Zwiers, F. W., and H. von Storch, 1995: Taking serial correlation into account in tests of the mean.
622 *Journal of Climate*, **8** (2), 336–351, doi:10.1175/1520-0442(1995)008<0336:TSCIAI>2.0.CO;2,
623 URL [https://doi.org/10.1175/1520-0442\(1995\)008<0336:TSCIAI>2.0.CO;2](https://doi.org/10.1175/1520-0442(1995)008<0336:TSCIAI>2.0.CO;2), [https://doi.org/10.](https://doi.org/10.1175/1520-0442(1995)008<0336:TSCIAI>2.0.CO;2)
624 [1175/1520-0442\(1995\)008<0336:TSCIAI>2.0.CO;2](https://doi.org/10.1175/1520-0442(1995)008<0336:TSCIAI>2.0.CO;2).

625	LIST OF FIGURES	
626	Fig. 1.	Locations of the automatic weather stations used in this study. Stars indicate capital city airport stations. Height and depth shading intervals every 200 and 1000 m, respectively. 31
627		
628	Fig. 2.	Heatmaps of \overline{WPI} values and confidence scores for each coastal station group and hour of the day: a) and b), Official versus ACCESS, c) and d) Official versus ECMWF, e) and f) ECMWF versus ACCESS. Positive \overline{WPI} values mean that the former dataset in each pair is on average closer to observations than the latter dataset. Confidence scores provide the probability the population \overline{WPI} is greater than zero. Values within the heatmaps are accurate to two significant figures. 32
629		
630		
631		
632		
633		
634	Fig. 3.	Time series, a) and b), of \overline{wpi}_{OA} and \overline{wpi}_{OE} for, a), the NT station group at 23:00 UTC, and b), the south WA station group at 05:00 UTC. Hodographs, c) to f), showing change in winds, c) and e), and wind perturbations, d) and f), for the NT station group, c) and d), and south WA station group, e) and f). 33
635		
636		
637		
638	Fig. 4.	Hodographs showing change in winds with height at, a), Darwin Airport, and b), Perth Airport. 34
639		
640	Fig. 5.	The \overline{wpi}_{OE} (Official versus ECMWF comparison) values, a) and c), and confidence scores, b) and d), for the airport stations, a) and b), and airport station groups, c) and d), respectively. 35
641		
642	Fig. 6.	Climatological hodographs. 38
643	Fig. 7.	As in Fig. 5, but for the $cwpi$ values and confidence scores. 39
644	Fig. 8.	Could also provide an analogous figure showing the use of the function α provides a significant improvement over the basic ellipse fit - or instead just quote some numbers? Or maybe these figures are entirely unnecessary? 40
645		
646		
647	Fig. 9.	Ellipse fits. If we were to include any analysis for alternative time periods (e.g. summer 2017/18 for contrast; or could do 18/19 if I were to go back to BoM to get the data) a copy of this figure could be a good choice. Could explain changes in diurnal cycle properties, e.g. amplitude, with seasonal changes to background winds, heating, etc. Note some issues with timing and amplitude values due to asymmetry - could instead just show eccentricity and orientation values? 41
648		
649		
650		
651		
652		
653	Fig. 10.	Ellipse fits. Could instead just provide one example. 42
654	Fig. 11.	Ellipse fits. Could also include the ellipses, but this makes the figure very large. 43
655	Fig. 12.	Actual perturbation standard deviation values. Note that official performs the worst at this scale! 44
656		
657	Fig. 13.	Actual perturbation standard deviation values. Note that official performs the worst at this scale! 45
658		

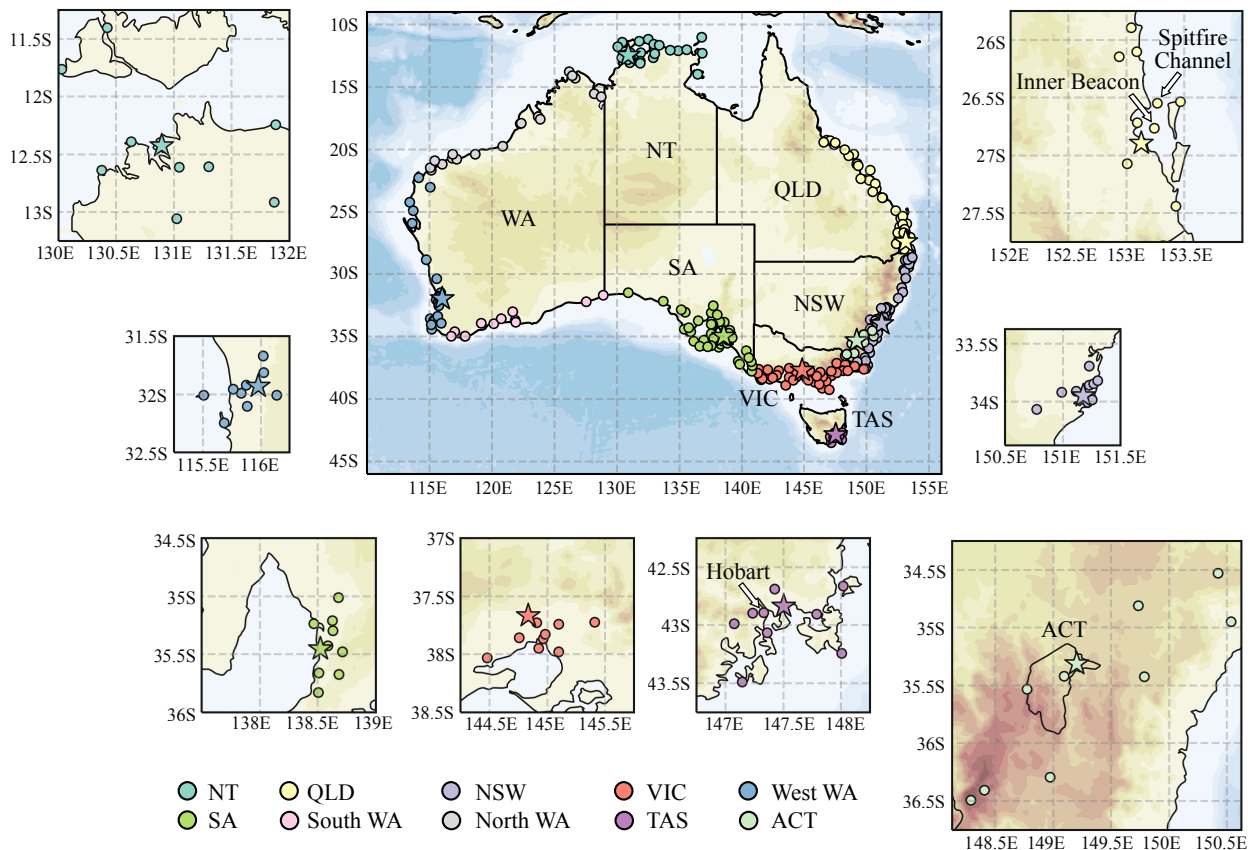


FIG. 1. Locations of the automatic weather stations used in this study. Stars indicate capital city airport stations. Height and depth shading intervals every 200 and 1000 m, respectively.

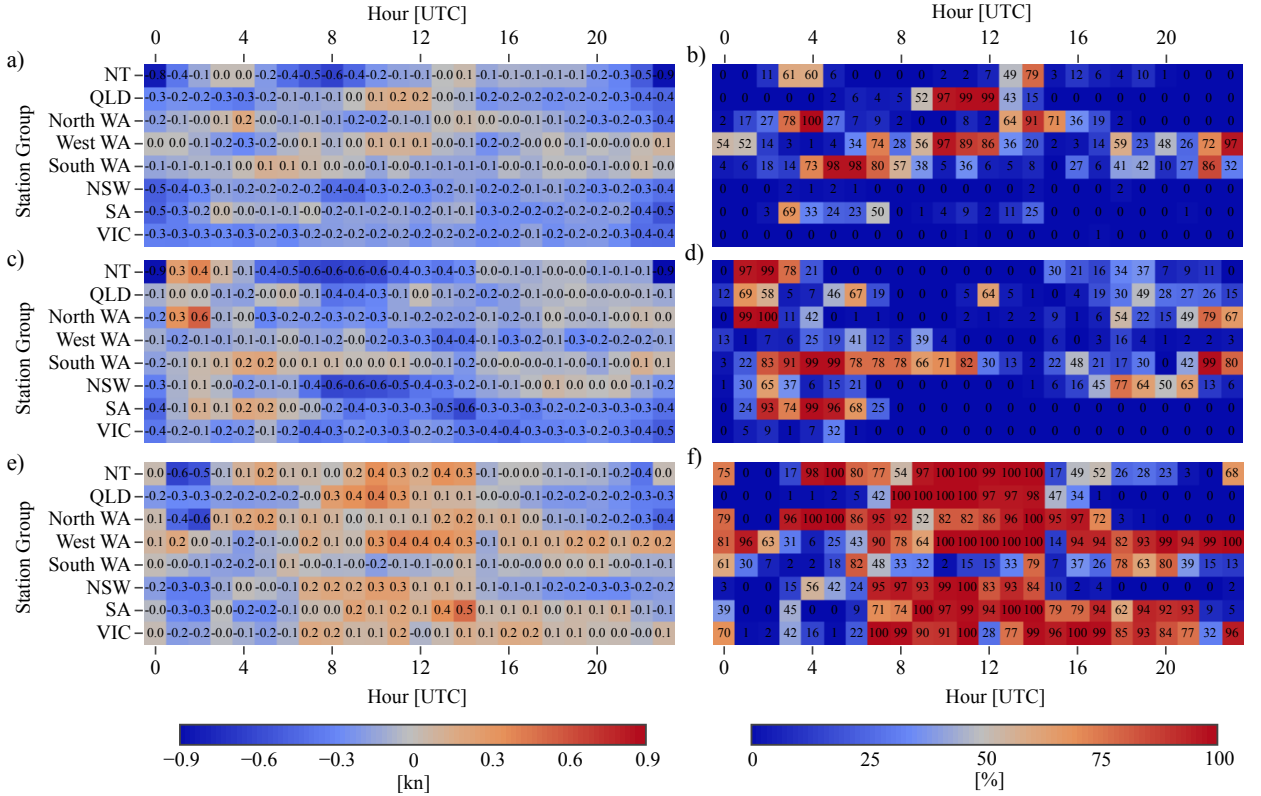


FIG. 2. Heatmaps of $\overline{\text{WPI}}$ values and confidence scores for each coastal station group and hour of the day: a) and b), Official versus ACCESS, c) and d) Official versus ECMWF, e) and f) ECMWF versus ACCESS. Positive $\overline{\text{WPI}}$ values mean that the former dataset in each pair is on average closer to observations than the latter dataset. Confidence scores provide the probability the population $\overline{\text{WPI}}$ is greater than zero. Values within the heatmaps are accurate to two significant figures.

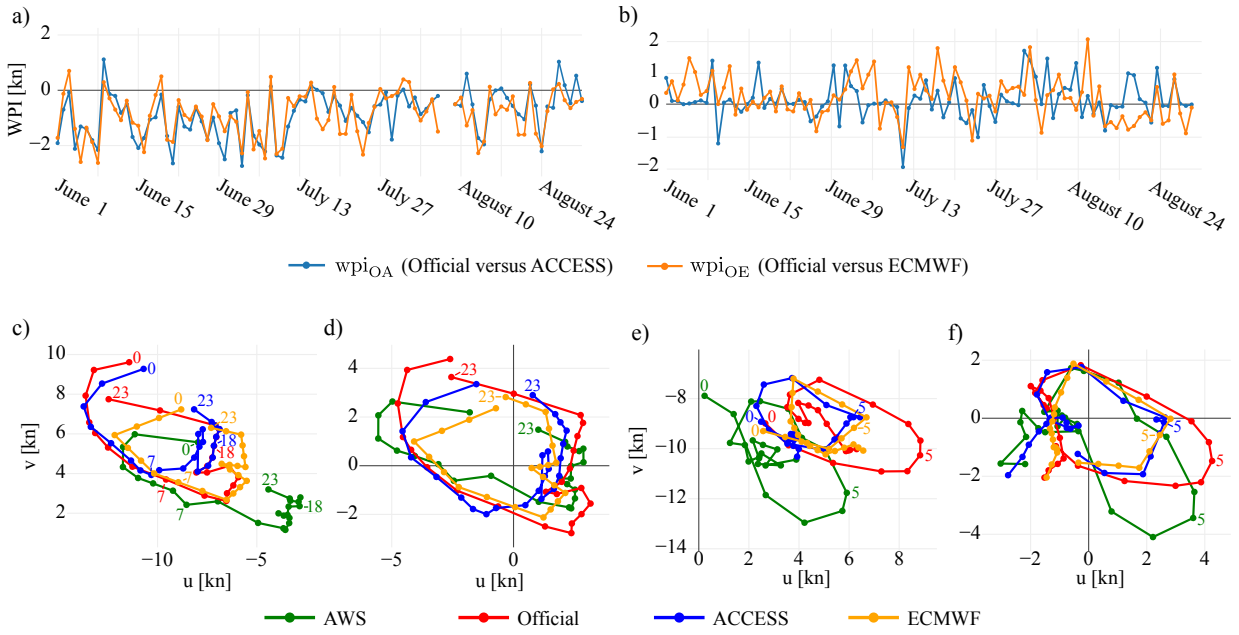


FIG. 3. Time series, a) and b), of \overline{wpi}_{OA} and \overline{wpi}_{OE} for, a), the NT station group at 23:00 UTC, and b), the south WA station group at 05:00 UTC. Hodographs, c) to f), showing change in winds, c) and e), and wind perturbations, d) and f), for the NT station group, c) and d), and south WA station group, e) and f).

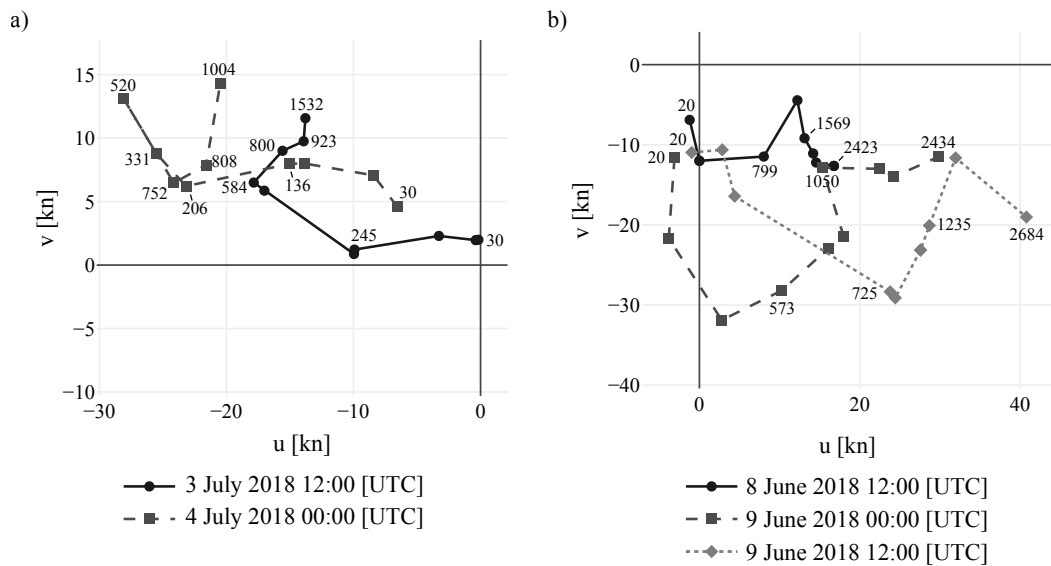


FIG. 4. Hodographs showing change in winds with height at, a), Darwin Airport, and b), Perth Airport.

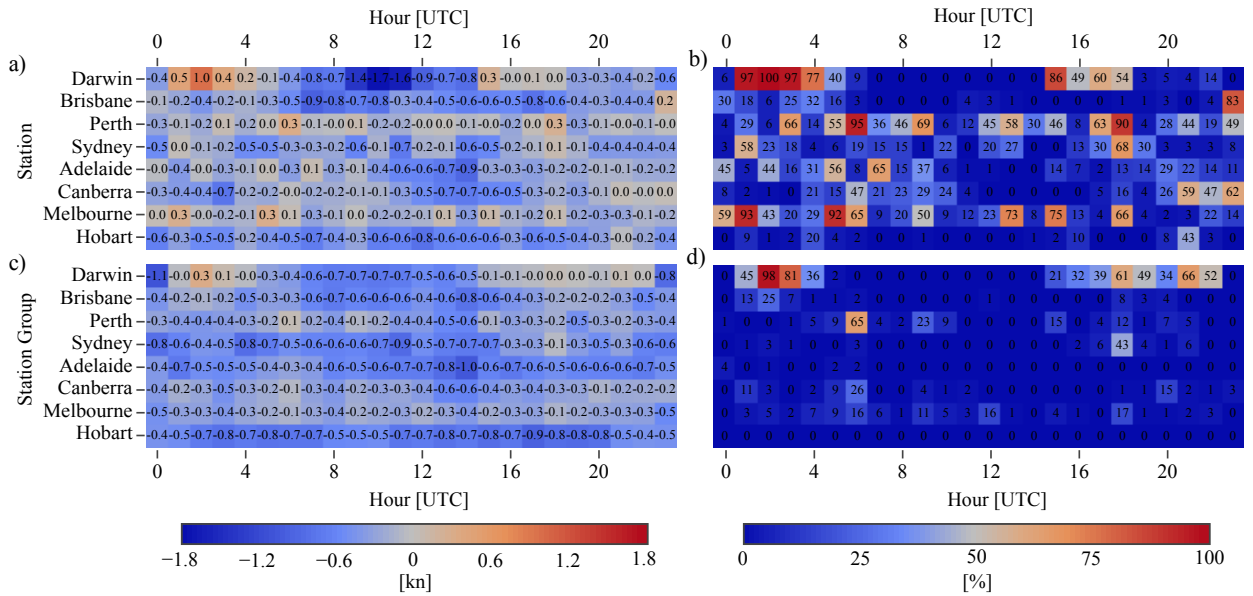
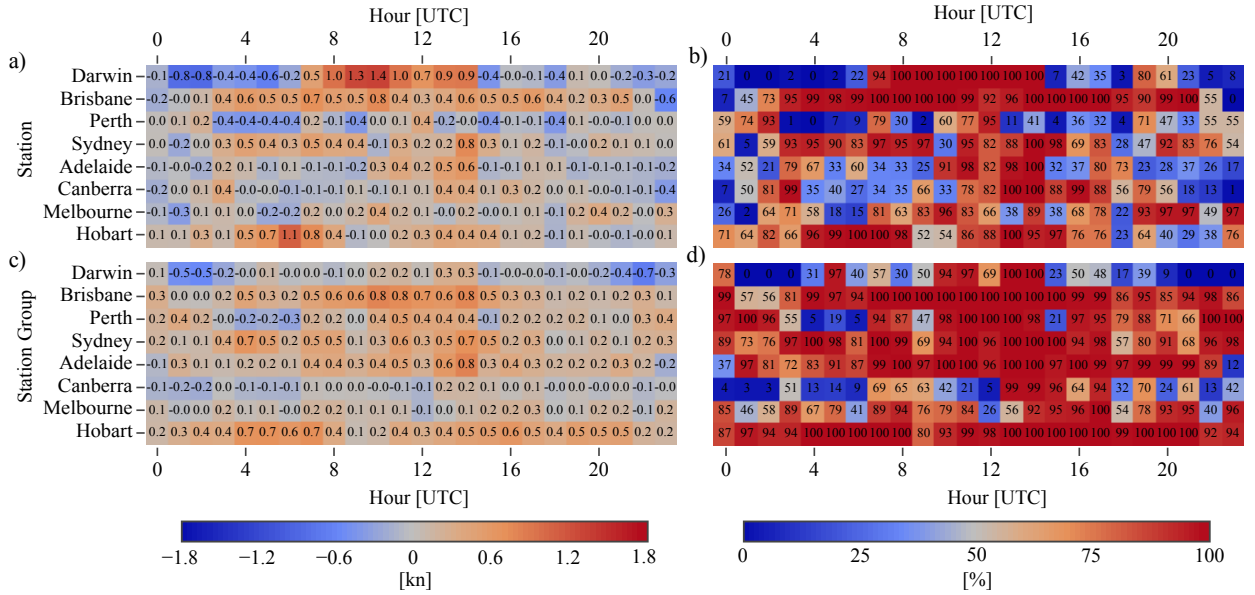
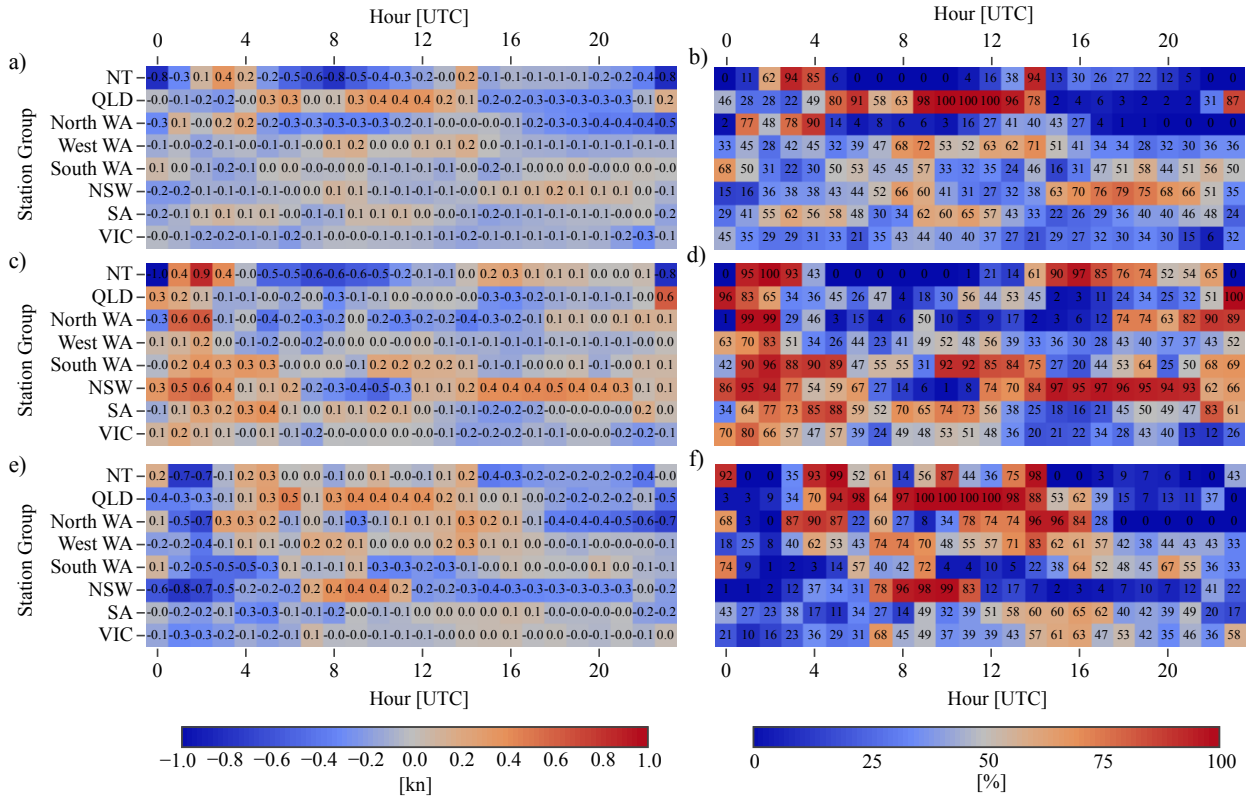


FIG. 5. The \overline{wpi}_{OE} (Official versus ECMWF comparison) values, a) and c), and confidence scores, b) and d),

for the airport stations, a) and b), and airport station groups, c) and d), respectively.





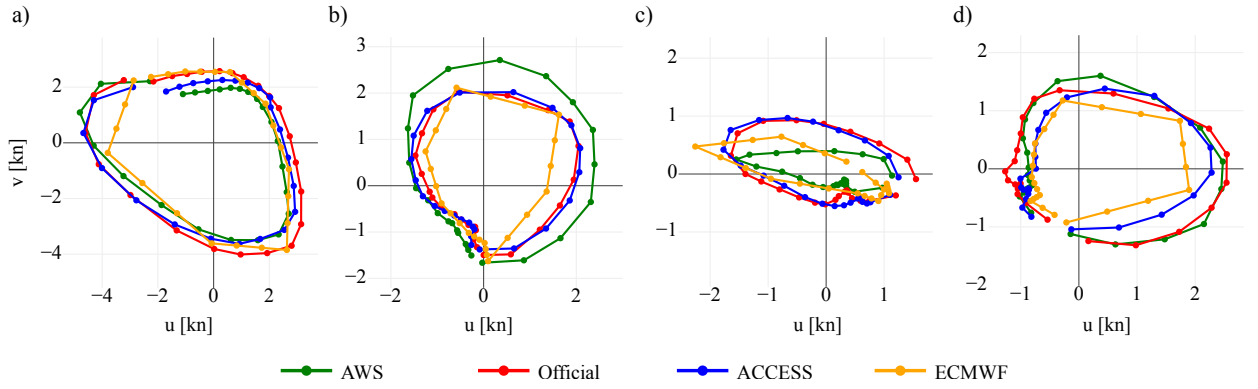


FIG. 6. Climatological hodographs.

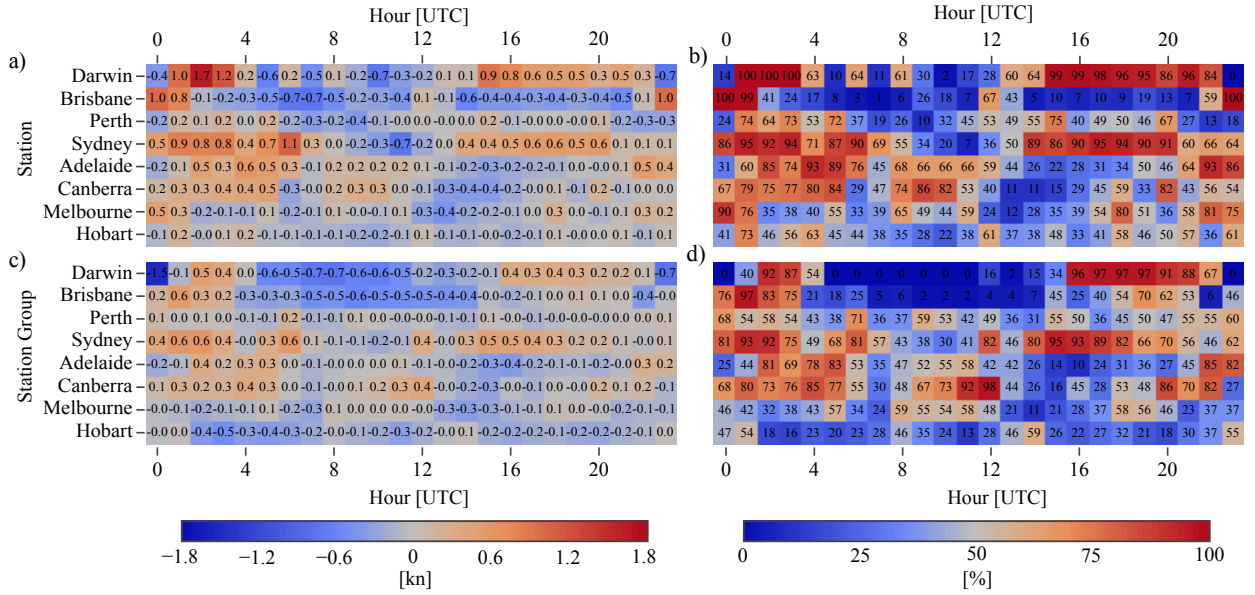


FIG. 7. As in Fig. 5, but for the cwpi values and confidence scores.

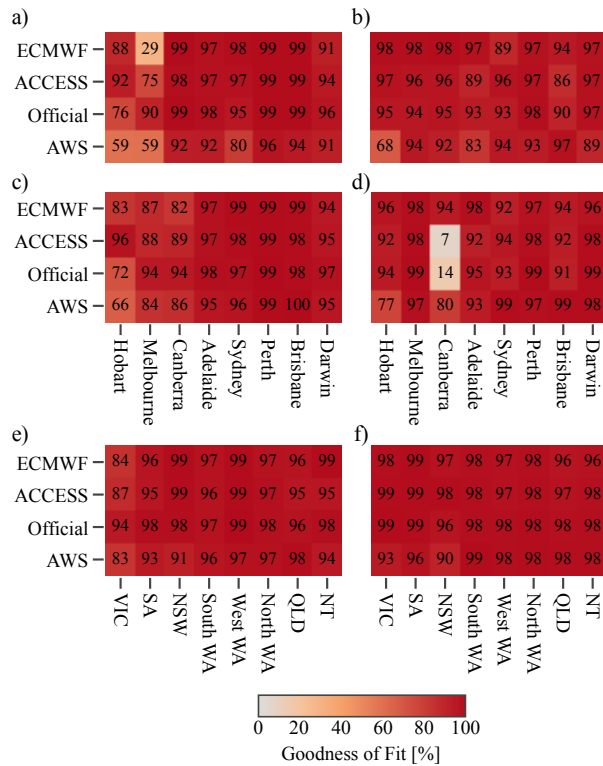


FIG. 8. Could also provide an analogous figure showing the use of the function α provides a significant improvement over the basic ellipse fit - or instead just quote some numbers? Or maybe these figures are entirely unnecessary?

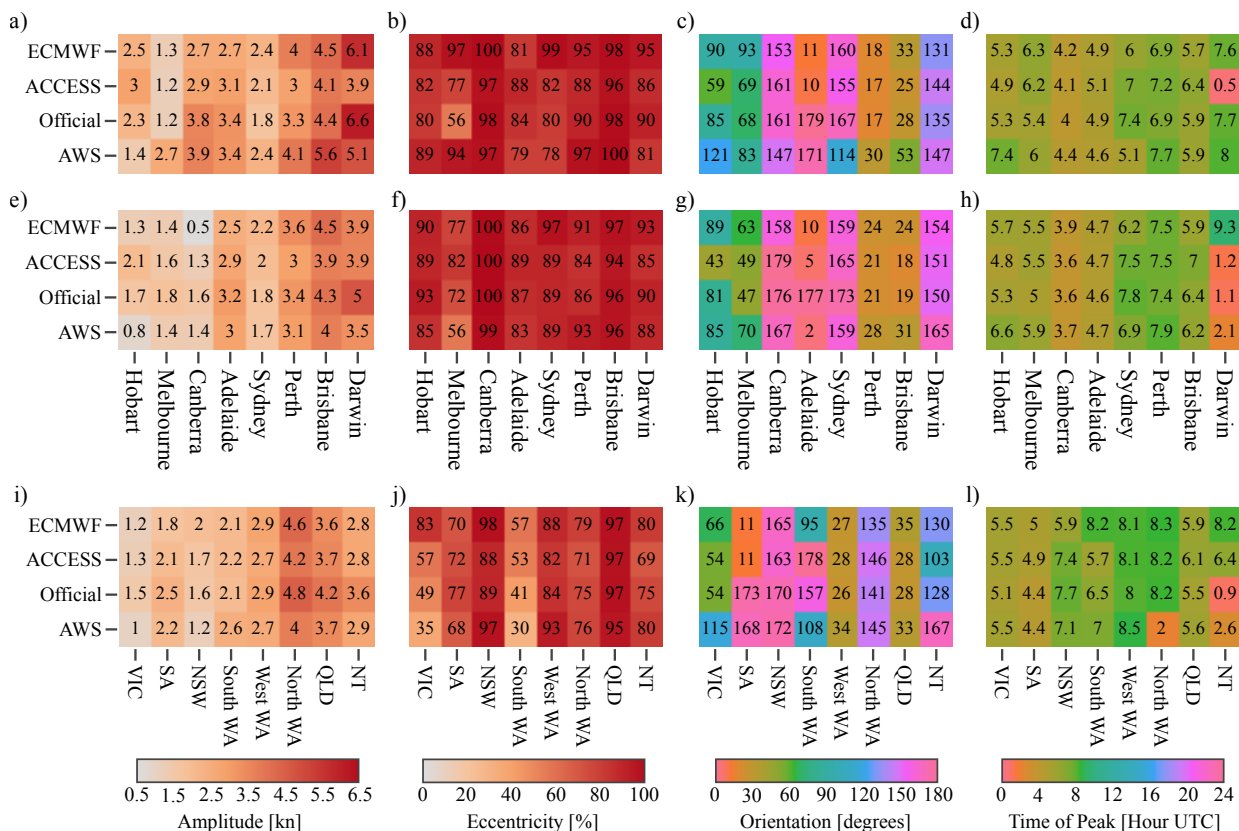


FIG. 9. Ellipse fits. If we were to include any analysis for alternative time periods (e.g. summer 2017/18 for contrast; or could do 18/19 if I were to go back to BoM to get the data) a copy of this figure could be a good choice. Could explain changes in diurnal cycle properties, e.g. amplitude, with seasonal changes to background winds, heating, etc. Note some issues with timing and amplitude values due to asymmetry - could instead just show eccentricity and orientation values?

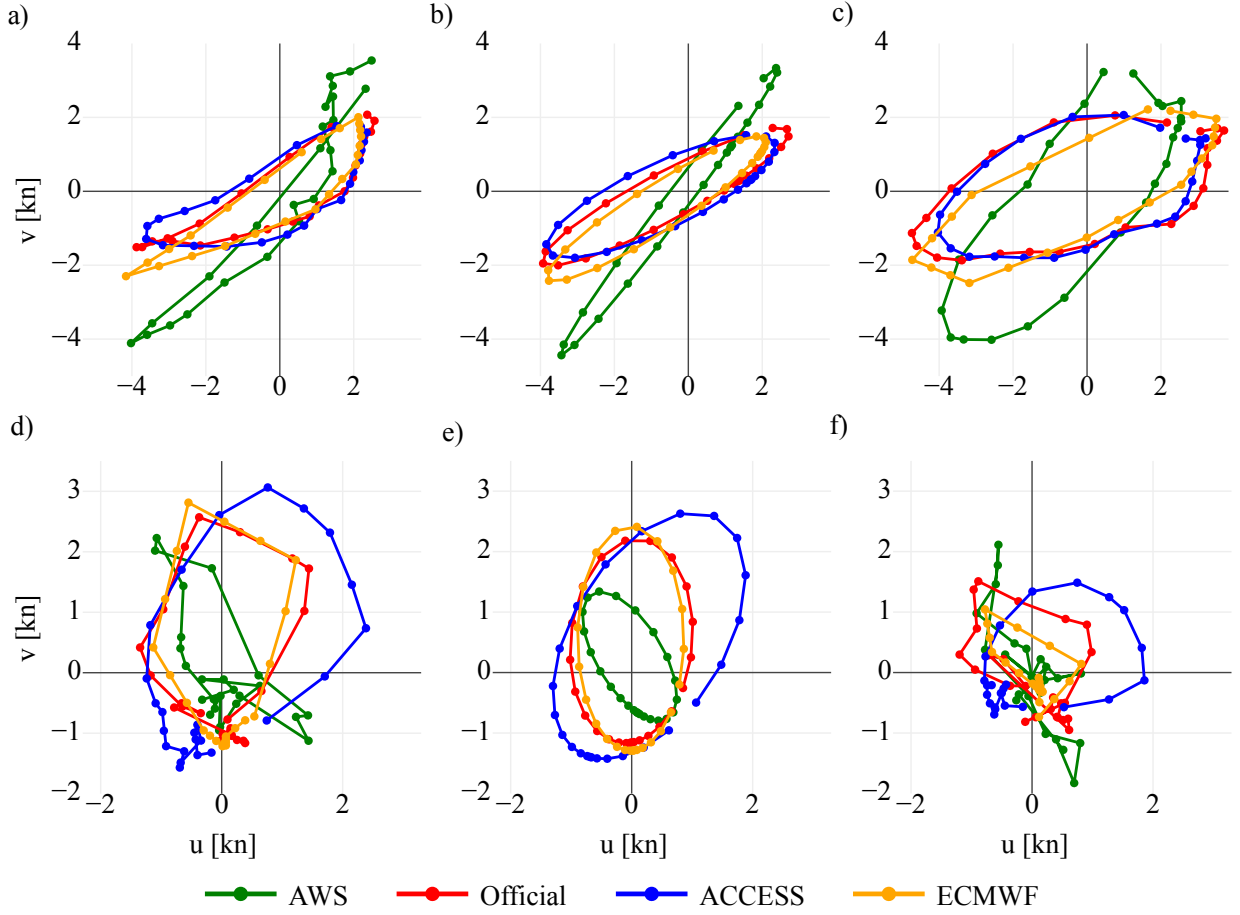


FIG. 10. Ellipse fits. Could instead just provide one example.

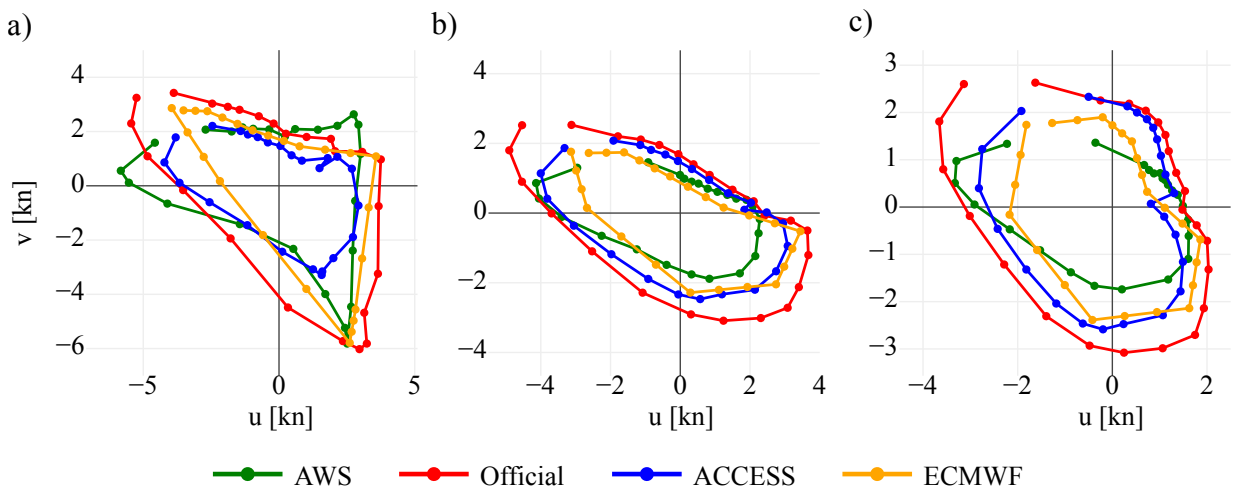


FIG. 11. Ellipse fits. Could also include the ellipses, but this makes the figure very large.

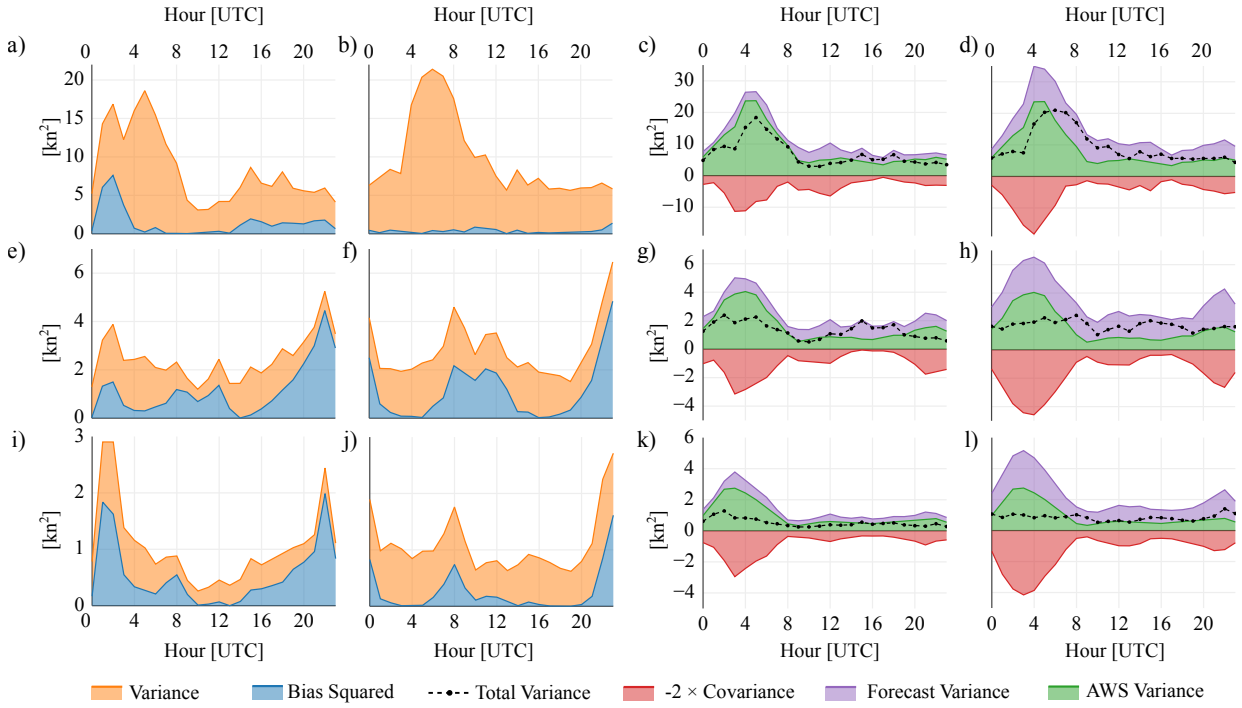


FIG. 12. Actual perturbation standard deviation values. Note that official performs the worst at this scale!

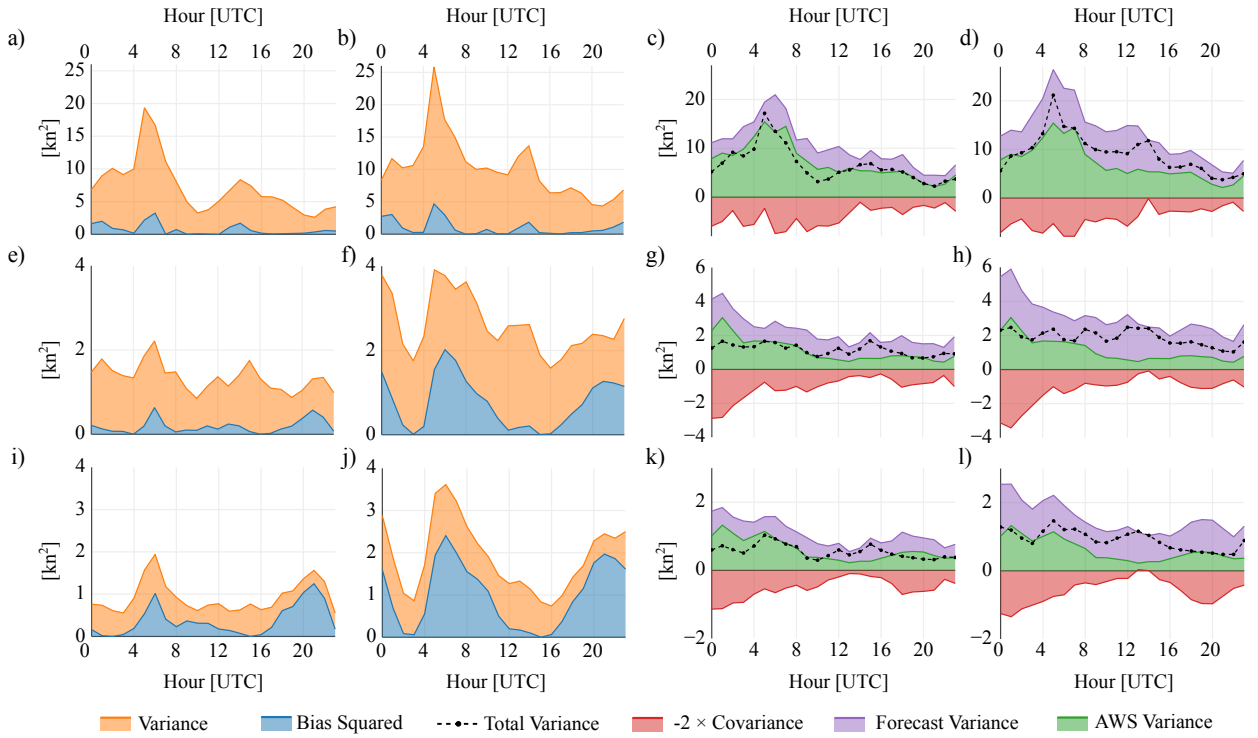


FIG. 13. Actual perturbation standard deviation values. Note that official performs the worst at this scale!